Chapter 11

Advanced Label-Free Optical Methods for Spermatozoa Quality Assessment and Selection

Annalisa De Angelis, Maria Antonietta Ferrara, Giuseppe Coppola and Anna Chiara De Luca

Additional information is available at the end of the chapter

http://dx.doi.org/10.5772/intechopen.71028

Abstract

Current *in vitro* fertilization (IVF) techniques require a severe selection of sperm, generally based on concentration, morphology, motility, and DNA integrity. Since routinely separation methods may damage the viability of the sperm cell, there is a growing interest in providing a method for noninvasively analyzing spermatozoa taking into account all those parameters. This chapter first reviews the state-of-the-art of label-free sperm cell imaging for IVF, highlighting the limitations of the used techniques. Then, our innovative approach combining Raman spectroscopy and digital holography will be described and its advantages detailed. These include the ability to perform a simultaneous and correlative morphological and biochemical analysis of sperm cells, without labeling, in a fast and reliable way. Finally, the difficulty in reaching clinical use will be discussed, as well as the possible solutions offered by new technological improvements.

Keywords: Raman spectroscopy, digital holography, sperm morphology, label-free analysis, sex-sorting

1. Introduction

It has been estimated that about 15–20% of couples worldwide have infertility problems or impaired fecundity. Approximately 40–50% of these cases are due to male infertility, which could be indirectly measured through the assessment of the sperm production and quality. According to WHO's criteria [1], indeed, men with low sperm concentration (oligospermia), poor sperm motility (asthenospermia), and abnormal sperm morphology (teratospermia) are considered to have male infertility factors. The revised WHO's parameters and the corresponding lower reference limits for semen analyses are reported in **Table 1**.

Infertile couple usually resort to assisted reproduction techniques (ART), chosen by the clinician according to the degree (soft, moderate, or severe) and kind (male and/or female) of

Parameter	Reference value	95% confidence index
Sperm volume	1.5 mL	1.4–1.7
Sperm concentration	15 million sperm/mL	12–16
Total sperm number	39 million sperm per ejaculate	33–46
Morphology	4% normal forms	3–4
Vitality	58% live	55–63
Progressive motility	32%	31–34
Total motility (progressive + nonprogressive)	40%	38–42

Table 1. WHO's parameters for semen analysis (2010).

infertility. For soft/moderate infertility, usually homologous intrauterine insemination (HIUI) or *in vitro* fertilization (IVF) is carried out. HIUI consists in transferring a small volume of selected and isolated motile and morphologically normal spermatozoa directly into the uterus a few hours before the ovulation. IVF is used after continued failures of HIUI due, for example, to an impervious uterine tube, and the fertilization of the oocytes takes place outside the woman body.

In case of severe male infertility, the intracytoplasmic sperm injection (ICSI) is preferred. In this technique, a single spermatozoon is directly injected into an oocyte, bypassing the physiological selection naturally performed by the female tract. Although ICSI has drastically reduced the number of viable sperm required for fertilization, giving hope of conception to extremely severe cases of oligospermia, the rate of successful pregnancy still remains low (<30%), due to the lack of accurate and reliable methods for selecting the spermatozoon that able to fertilize the oocyte.

The first selection is based on motility and morphology. The sperm cells preparation procedure includes a density gradient centrifugation (morphology-based selection) followed by swim-up method (motility-based selection) in order to mimic the physiological selection of the spermatozoa made by the female genital tract. In most laboratories, the sperm quality assessment is relied on the expertise and the subjective skills of the operator. To increase precision and reproducibility, numerous automated computer-aided sperm analysis (CASA) systems have been introduced, and they can automatically view multiple fields in a shallow specimen chamber to capture images of 500 to >2000 sperm in <2 minutes [2]. By using CASA, it is also possible to retrieve some morphometrical parameters, such as ellipticity and regularity, whereas the measurement of the acrosome area generally requires staining.

Moreover, CASA has difficulty in distinguishing spermatozoa from particulate debris, leading to some extent of inaccuracy. In addition, several studies have shown that the correlation between male fertility and the percentage of morphologically normal or motile sperm cells in semen sample is relatively low [3, 4]. Indeed, in infertile men, a high percentage of spermatozoa with a normal morphology or motility could have a damaged DNA, and therefore, they are, in principle, incapable to fertilize the oocyte [4, 5].

Sperm DNA integrity is generally assessed by biochemical methods such as terminal deoxynucleotidyl transferase dUTP nick end labeling (TUNEL) assay [6], comet assay [7], sperm chromatin dispersion (SCD) test [8], or sperm chromatin structural assay (SCSA) [9], which assess the quality of DNA bases, chromatin, and altered protein in sperm nuclei using specific stains. Indeed, all currently employed tests to determine DNA integrity are of limited clinical utility as they are invasive and destructive, rendering the sample unusable for IVF [6–11].

All these methods mentioned above, only based on assessing morphology or motility, are inadequate to select the fertile spermatozoon as the selection techniques have to be noninvasive, safe, highly discriminative, and relatively easy to perform. Moreover, they should simultaneously assess three conditions: normal morphology, motility, and DNA integrity.

Recently, several techniques are emerging for label-free selection of viable spermatozoa. In this chapter, we focus on two of them: Raman-based spectroscopy and phase contrast imaging. Raman spectroscopy (RS) investigates the biochemical and physiological state of a sample by detecting the inelastic light scattering, without labeling or long preparation procedures [12]. Phase contrast imaging includes basic microscopies (bright-field) [13] and more advanced ones (interferometric microscopies) [14–17], such as digital holography. These methods exploit the phase delay of light when passing through a sample. Then, these light delays are converted into intensity changes and recorded on a camera as holograms containing the information suited for morphological sperm cell reconstructions.

The physical principles and the technical instrumentation of Raman and holographic techniques will be separately described in Sections 2 and 3, respectively, also highlighting some relevant results in sperm cells analysis. In Section 4, we will report on our recent achievements using the two techniques in a multimodal analysis setting. Indeed, both the techniques are based on intrinsic optical properties of the sample and may offer the unique advantage to simultaneously acquire the holographic and Raman data assessing single spermatozoa on the base of their morphological and biochemical parameters and their motility. The complete analysis is performed by the same optical system, with a strong impact on costs and times for the analysis. This aspect makes the proposed approaches very promising for clinical applications; however, at present, they are only in experimental stages and specific recommendations for routine procedures cannot be made. At the end of this chapter, the difficulty in reaching clinical use will be discussed, as well as the possible solutions offered by new technological improvements.

2. Label-free biochemical sperm analysis

2.1. Basic principles of Raman spectroscopy

Raman spectroscopy is an optical technique based on the scattering of the light interacting with a sample. Light scattering originates from the elastic or inelastic collision between an incident photon and a molecule of the sample. When the collision occurs, the molecule undergoes an excitation to a virtual state followed by a nearly simultaneous de-excitation towards the initial energy level (elastic) or a vibrational level different from the initial one

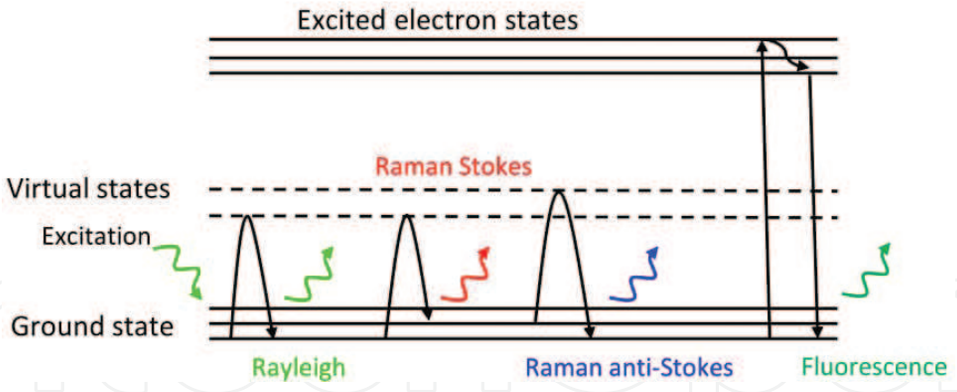

Figure 1. Jablonski diagram representing quantum energy transitions for Rayleigh, Raman scattering (Stokes and anti-Stokes), and fluorescence emission.

(inelastic) (**Figure 1**). The virtual state is an energy level created only when photons interact with electrons and its energy is determined by the frequency itself of the incident photons. When molecules return back to their initial energy state, photons are emitted (scattered). In the elastic process, named Rayleigh scattering, the emitted photons have the same energy of the incident ones. Whereas in the inelastic scattering, there are two possibilities (**Figure 1**): 1. molecules decay from the virtual state to an excited vibrational level emitting photons with a lower energy than the incident ones (Stokes scattering) and 2. when molecules in a vibrational state were excited in a virtual state, they can decay in the ground state, producing photons with energy higher than the incident ones (anti-Stokes scattering). Since the number of molecules in an excited state decreases very fast, anti-Stokes scattering is much less probable than the Stokes scattering (typically by a factor around 1000). For this reason, Raman analysis is usually limited to the observation of the Stokes scattering.

The energy difference between the initial and final vibrational levels (Raman shift) expressed in wavenumbers (cm^{-1}) is given through the relation:

$$\hbar\nu = \hbar\left(\frac{1}{\lambda_{inc}} - \frac{1}{\lambda_{scat}}\right) \tag{1}$$

in which λ_{inc} and λ_{scat} are the wavelengths of the incident and Raman scattered photons, respectively. Therefore, the energy (or frequency) shifts in the scattered radiation provide a direct measure of the vibrational frequencies of the molecule (ν). Since different molecules are characterized by defined vibrational modes, by collecting the photons scattered at different frequencies allows reconstructing a sort of "chemical fingerprint" of the sample.

Therefore, RS turns out to be an extremely powerful tool for interdisciplinary researches, involving physicists, chemists, and biologists, as it allows the characterization of molecules based on properties of chemical bonds. It is a noninvasive and nondestructive technique providing molecular-level information, allowing the investigation of functional groups, bonding types, and molecular conformations.

From an experimental point of view, to observe a Raman spectrum, it is required to suppress the light scattered at the same frequency of the incident radiation (Rayleigh scattering), often

more intense than the Raman scattering. Using the notch filter, disperse the spectral components of the light by means of the diffraction grating and image the light onto the detector (high sensitive charge-coupled device (CCD) camera).

In a confocal configuration (micro-RS), a spatial resolution of ~300 nm in the transverse x-y plane and of ~1.2 μm in the axial direction can be achieved. Moreover, for extended samples, it is possible to acquire the Raman spectra on a two- or three-dimensional array of points, scanning the sample with a step comparable with the spatial resolution (Raman imaging). In this way, 2D images (or 3D profiles) are obtained, reporting the spatial variation of a given Raman parameter. This parameter is usually the intensity of a particular Raman band or sometimes it derives from a more complicated analysis of the whole Raman spectrum [18, 19].

2.2. Raman spectroscopy analysis of sperm cells quality

Interestingly, due to the cited characteristics, RS has been successfully employed for the study of several living/fixed cells with subcellular resolution [18]. The first Raman-based single cell analyses were conducted just on individual living salmon sperm cells due to their relative simple structure [20]. Since this pioneer study, no other Raman experiments on sperm cells have been reported until the 2009 when Huser and colleagues [21] examined the spectra obtained from human spermatozoa with different nuclear shapes (box 1 in **Figure 2**) in order to determine if there was a correlation between DNA-protein complex in sperm chromatin and the morphology of the nucleus. RS results showed that while the DNA packaging of normal and abnormal shaped nuclei was different, the nature and the efficiency of DNA packaging in normal head spermatozoa appeared to vary greatly [21]. Therefore, by selecting sperm cells solely based on morphology, a fraction of the normal considered sperm cells used for *in vitro* fertilization will contain improperly packaged DNA, thus resulting infertile. In this study, fixed membrane-free cells were used in order to minimize the potentially interfering contributions from membrane proteins.

The results of this study are also relevant from an epigenetic point of view. Indeed, they show the possibility to use RS for detecting epigenetic alterations (DNA packaging and spatial conformation, methylation and histone modification) in those spermatozoa that, if used in assisted reproductive techniques, may increase the incidence of imprinting disorders and have a deleterious impact on embryonic development [21, 22].

In other studies, RS was applied on whole and fixed sperm cells in order to demonstrate the efficiency of the technique in identifying DNA-damaged sperm cells (box 2 and panels A and Z in the box 3 of **Figure 2**). Usually, the DNA fragmentation as a consequence of oxidative stress is induced by UV radiation [23, 24] or Fenton's treatment [25]. All the studies found that the PO_2 backbone of DNA was significantly affected by the exposure to radiation or treatment, and thus, its corresponding Raman band could represent a significant biomarker of DNA fragmentation [23–25]. Mallidis et al. previously identified characteristic spectral changes indicative of nuclear DNA damage of single fixed human spermatozoa and using Raman mapping, they localized the most damaged sites [24].

In the following study [25], the same group determines the possibility to use Raman microspectroscopy for identifying different levels of sperm nuclear DNA damage induced by oxidative

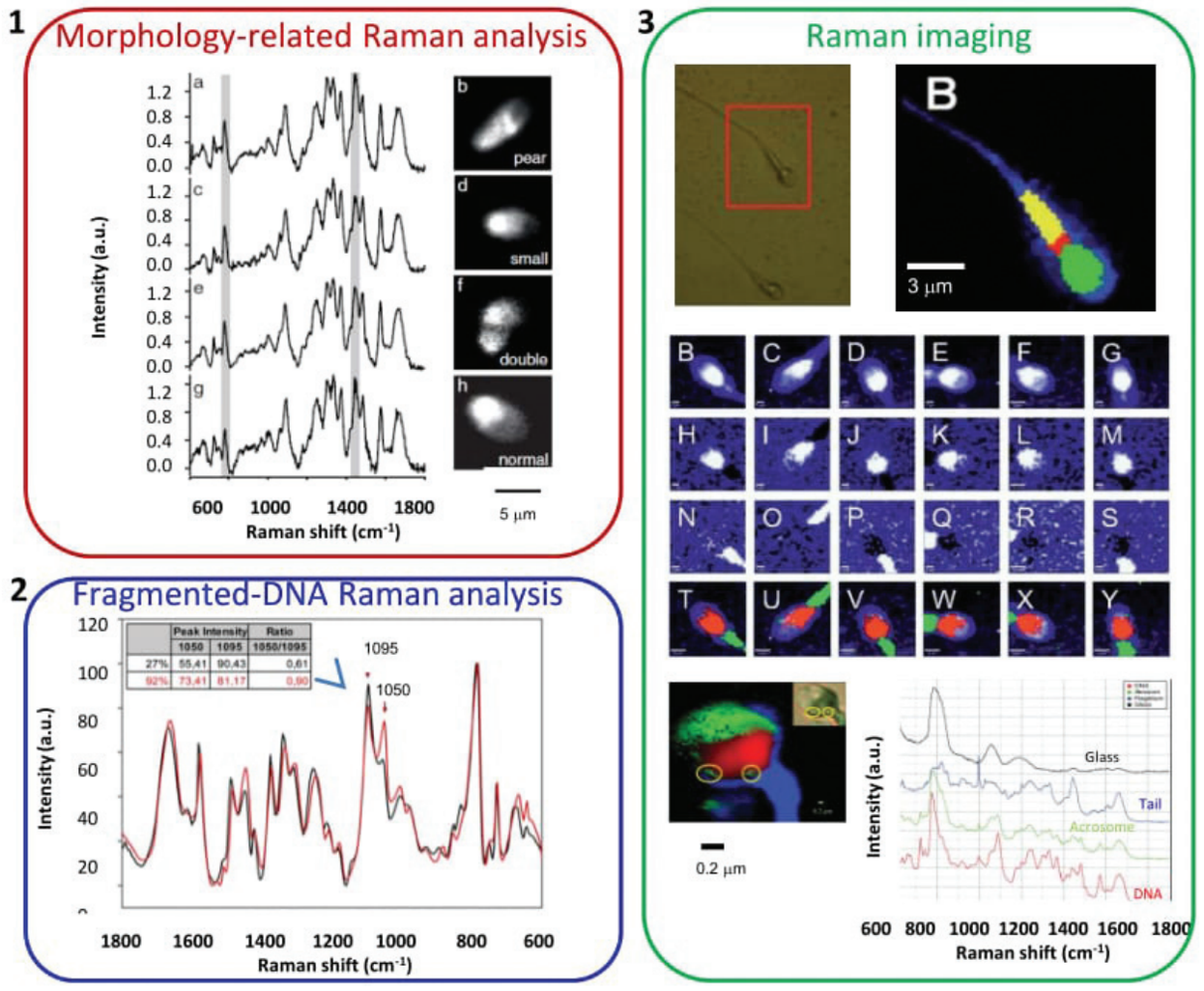

Figure 2. Overview of the most representative studies on Raman spectroscopy and imaging for the label-free analysis of sperm cells. Box 1: the highlighted variations in peak intensities in the Raman spectra correspond to different sperm head shapes [21]. Box 2: the peaks at 1095 and 1050 cm^{-1} represent biomarkers of fragmented DNA in the sperm nucleus [24, 25]. Box 3: panel A shows the chemical Raman reconstruction of distinct sperm regions [23]; panels B–Y represent the biochemical composition of individual immobilized, living human sperm cells [26]; and panel Z shows the efficiency of Raman imaging in revealing small irregularities in the sperm head such as vacuoles (yellow circles) distinguishable based solely on the presence of differing spectra [24].

stress and corroborated the findings using an established assay and an alternative but complementary spectroscopic technique (Fourier-transform infrared (FTIR) spectroscopy). The results of this last work confirm that RS is able to reveal different levels of oxidative DNA fragmentation, especially associated to alterations within the 1050–1095 cm^{-1} spectral range (Raman spectra in the box 2 of **Figure 2**), which includes the band associated with the DNA phosphate backbone, changes that were confirmed by similar shifts in the corresponding FTIR peaks (not shown) [25]. Also, the Raman bands associated to protein and lipid content (1400–1600 cm^{-1}) showed some alterations induced by UV radiation, consistent with protein denaturation and lipid peroxidation that are well-known markers of oxidative damage [27]. Raman-based identification of DNA-damaged sperm cells linearly correlated with the findings from the flow

cytometric analysis of DNA fragmentation, which represents the most statistically robust, reproducible, and standardized procedure available for the determination of sperm nDNA damage [28].

In 2015, Edengeiser et al. [26] analyzed spermatozoa under near-physiological conditions using confocal Raman microspectroscopy. The spermatozoa are immobilized on pre-treated object slides. More in detail, CaF_2 slides were coated with concanavalin A and overlaid with preheated Ringer's solution just before putting a drop of isolated spermatozoa which, after the analysis, can be easily removed from the substrate. The study demonstrated for the first time the possibility to image and analyze several tens to hundreds individual cells with a rate of one cell per minute with submicrometer resolution (panels B–Y in the box 3 of **Figure 2**). This opens up possibilities to investigate different physical and biochemical parameters under physiological conditions, leaving the assessed spermatozoa functional.

3. Quantitative phase imaging for sperm analysis

3.1. Basic principles of quantitative phase microscopy

Quantitative phase microscopy (QPM) is a label-free imaging technique, which allows reconstructing both the amplitude and the phase information of an optical field that passes through the sample, and it is particularly interesting in case of transparent biological cells. Respect to differential interference contrast (DIC) microscopy [29] or Nomarski/Zernike's phase contrast [30], the QPM gives a quantitative measure of the optical path difference (OPD) at each point in the sample. OPD in each position (x, y) of the acquisition plane is defined as the refractive index variation across the cell thickness, $t(x, y)$:

$$OPD(x,y) = t(x,y)(n_c - n_s) \tag{2}$$

where n_c and n_s are the refractive index of the cell and the surrounding medium (assumed to be homogeneous), respectively. The resulting OPD map of the cell is reconstructed by recording the interference fringes pattern, the so called "hologram," of two superimposed coherent beams, one that interacts with an object under test and another that does not come in contact with the object and acts as a reference beam, and calculating the phase difference between them [31]. If the hologram is acquired by a digital sensor array, typically a charge-coupled device (CCD) or a complementary metal-oxide semiconductor (CMOS) device, digital holographic microscopy (DHM) technique is implemented. A typical interferometric setup for DHM is reported in **Figure 3**.

The acquired hologram is then mathematically analyzed, allowing obtaining the complex field of the object beam that can be reconstructed at different distances, too. Therefore, numerical refocusing of a digital hologram, that is a 2D image, at different object planes, without any z-scan of the optical system, allows to retrieve a 3D quantitative imaging [31]. This makes digital holography a very powerful method for metrology applications, particularly attractive in the field of biology as it is noninvasive, noncontact, and label-free, allowing the characterization of live specimen.

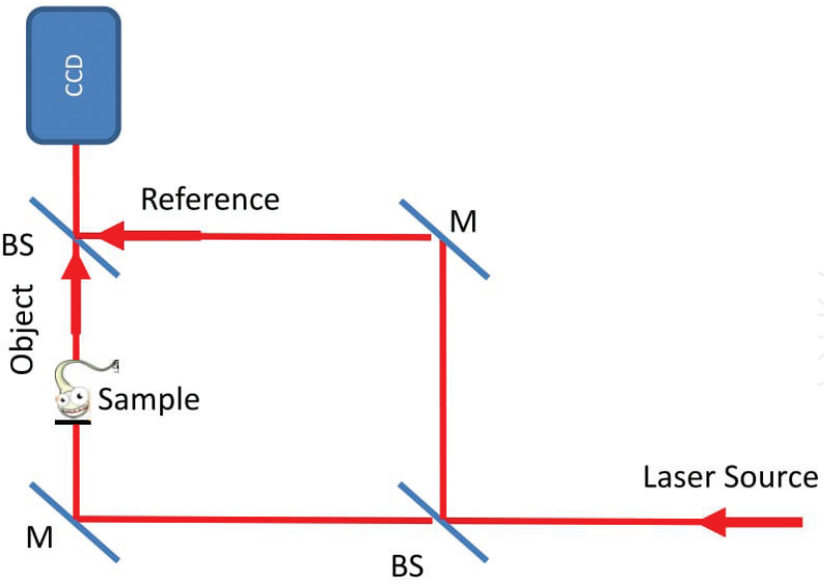

Figure 3. Typical interferometric setup for digital holography microscopy. BS: beam splitter, M: mirror. Reference and object beams are highlighted.

In DHM, in addition to the hologram of the sample under investigation, a second hologram is acquired on a reference region near to the object in order to numerically compensate all the aberrations due to the optical components, comprising the defocusing due to the microscope objective. An "off-axis" configuration is generally adopted to avoid a spatial overlapping of the real and conjugate images due to the holographic reconstruction, leading to the separation of first diffraction order from the entire spatial frequency spectrum. Thus, the spectrum of the sample (object field defined as $S(x,y) = |S(x,y)|e^{i\varphi(x,y)}$, with $|S(x,y)|$ and $\varphi(x,y)$ amplitude and phase, respectively) can be retrieved except for a constant [32]. Then, it is possible to propagate the optical wavefront at different distances from the plane of acquisition applying the Fourier formulation of the Fresnel-Kirchhoff diffraction formula [33, 34]. This reconstruction can be obtained by means of the operator algebra proposed by J. Shamir [35], where Fresnel diffraction is described by replacing the Fresnel-Kirchhoff integral, the lens transfer factor, and other operations by operators. The resulting propagated object field $S_{prop}(\xi,\eta)$ is expressed as a function of the initial object field $S(x,y)$ and can be written as [36, 37]:

$$S_{prop}(\nu,\mu) = \exp(ikd) \times \left\{ \Im^{-1}\left[\exp\left(-\frac{ikd\lambda^2}{2}\left(p^2+q^2\right)\right)\right] \cdot \Im(S(x,y)) \right\} \tag{3}$$

being $\Im[f(x)]$ the Fourier transform of the function $f(x)$, $k = \frac{2\pi n}{\lambda}$ (with n refractive index of the medium), p and q spatial frequencies defined as $p = \frac{\nu}{\lambda d}$ and $q = \frac{\mu}{\lambda d}$, and d the reconstruction distance. For digital reconstruction, Eq. (3) is applied in a discrete form:

$$S_{prop}(m,n) = \exp(ikd)\left\{ \Im_D^{-1}\left[-\frac{ikd\lambda^2}{2N^2d^2}\left(U^2+V^2\right)\right] \cdot \Im_D(S(h,j)) \right\} \tag{4}$$

where N is the number of pixels in both directions and m, n, U, V, h, and j are integer numbers varying from 0 to $N-1$.

Intensity and phase distributions can be reconstructed by $S_{prop}(m, n)$ according to the following equations:

$$I_{prop}(m,n) = \left|S_{prop}(m,n)\right|^2; \tag{5}$$

$$\varphi_{prop}(m,n) = \arctan\frac{\mathrm{Im}\left[S_{prop}(m,n)\right]}{\mathrm{Re}\left[S_{prop}(m,n)\right]}. \tag{6}$$

The phase $\varphi_{prop}(m, n)$ includes information about the morphological profile of the object under investigation; in fact, it is related to the *OPD*:

$$OPD(m,n) = \frac{\lambda}{2\pi}\varphi_{prop}(m,n). \tag{7}$$

The relation between the *OPD* and the thickness of the cell t is given by Eq. (2).

3.2. Digital holography microscopy for sperm cells assessment

Digital holography (DH) allows retrieving a fully 3D image of the sample, thus offering new prospects for the analysis of sperm cells in a noninvasive, quantitative, and label-free way. Sperm cells were acquired by a digital holographic microscope for the first time in 2008 by Mico et al. [38].

The potential of applying this technique for label-free sperm assessment was recently confirmed by Shaked's group. Indeed, they demonstrated that DHM allows obtaining equivalent information about key morphological parameters of fixed human spermatozoa to that obtained by bright field microscopy (BFM) imaging of stained sperm cells [39].

Additionally, the opportunity to have information about the third dimension in the sperm analysis can offer a better understanding of this kind of cell and of male infertility [40]. Furthermore, since this technique allows obtaining quantitative information and numerical analysis, estimation area or profiles in a given direction may be carried out. Such kind of analysis can help to study the male infertility and its possible relation with the abnormal morphology [41, 42].

DH has been mainly employed to study the morphology of human sperm cells in order to verify the integrity of their structures and to evaluate their kinematic parameters and concentration. This approach allows to visualize the morphology of abnormal sperm and to analyze in 3D some typical defects such as cytoplasmic droplet along the tail, bent tail, and acrosome broken, as reported in the box 1 of **Figure 4** [42].

Additionally, a quantitative study of vacuoles has been performed by DH. In particular, it was demonstrated that the profile of the normal spermatozoon results higher than that of the spermatozoon with vacuoles, whereas their 2D dimensions (such as area and axes length) are similar [43]. The difference in height denotes a reduced volume in spermatozoon with vacuoles respect to the normal spermatozoon; this difference could be ascribed to a modification of the inner structure of the sperm head with loss of material (see box 1 in **Figure 4**).

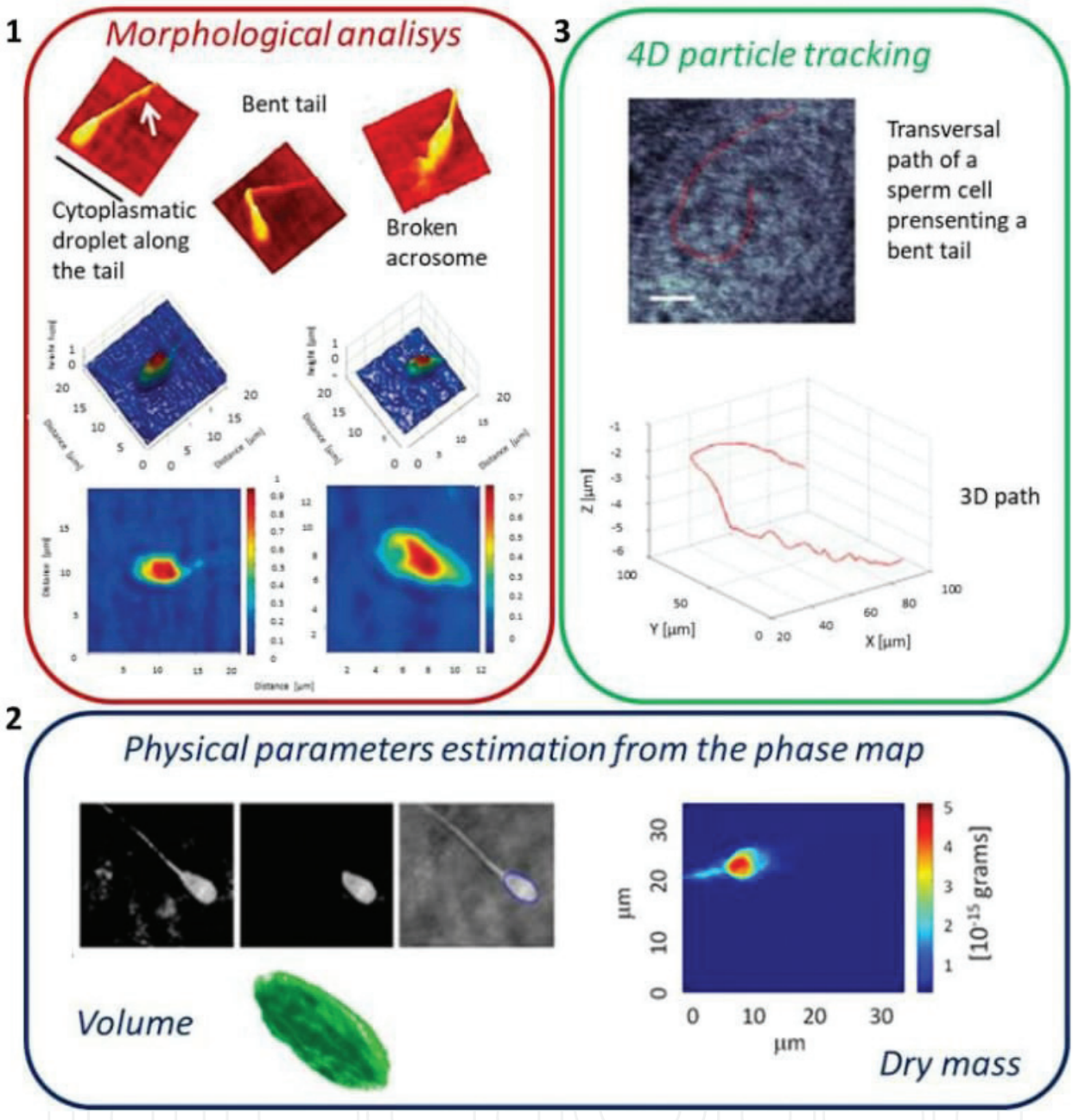

Figure 4. Some potentialities of DHM. Box 1: morphological analysis of semen carried out by DHM; top panels: sperm cells with distinct morphological defects; center and bottom panels: difference in height denotes a reduced volume in spermatozoon head with vacuoles respect to the normal spermatozoon [41, 43]. Box 2: examples of some physical parameters obtained by DHM [31, 44]. Box 3: 4D tracking of clinical sperm samples [45].

In 2013, Merola et al. [44] provided an evaluation of the biovolume of spermatozoa (about 55 μm^3). The authors used optical tweezers to trap and rotate the cells; meanwhile, they flow through a microchannel, enabling recording digital holograms of the sperm at different angles and the production of a tomographic 3D model, as showed in the box 2 of **Figure 4**.

Another important semen parameter, the dry mass of the cell (i.e. the average mass of the proteins, carbohydrates, lipids, and so on within the cell), can be obtained by DHM. Indeed,

the *OPD* of the cell linearly depends on the axially averaged refractive index of the cell relative to the surrounding medium, for a given thickness t [45]. Thus, considering that the human spermatozoa head can be divided in the cell nucleus and the acrosome, which differ in the composition and concentration of proteins, nucleic acids, and other components, Balberg et al. evaluated the dry mass of the cell by starting by the knowledge of the *OPD* [31]. In particular, the authors measured the dry mass of separate cellular compartments in the *OPD* maps of unlabeled human spermatozoa, as reported in the box 2 of **Figure 4**.

Finally, the movements of living spermatozoa have been tracked applying an automatic 4D tracking (movements in the 3D spatial directions over time) of the swimming samples in [46]. The results are showed in the box 3 of **Figure 4**, where an anomalous spermatozoa behavior, known as "bent tail," is highlighted. A collection of several holograms at a fixed distance between the sample and the microscope objective was acquired. In order to simultaneously track multiple spermatozoa, a proximity criterion has been included into the algorithm. In particular, by means of this approach, the position in the $(n + 1)$th frame has been searched in a reasonable neighborhood of the nth frame position.

Therefore, DH could be seen as a breakthrough that can renew the sperm analysis in the spermatology laboratories, encouraging researchers in the field of sperm cell biology to consider using DH as a standard method for their characterization studies.

4. Combined optical approach for the noninvasive analysis of single spermatozoa

As seen in the previous sections, Raman spectroscopy and quantitative phase microscopies have been separately developed for assessing spermatozoa from a biochemical and morphological perspective, respectively. The two photonic techniques, employing intrinsic contrast mechanisms, allow noninvasively selecting the fertile spermatozoon according to its normal morphology as well as its DNA integrity. Kang et al. [47] first proposed a combined system where quantitative phase microscopy and Raman imaging allowed correlating morphological parameters with molecular information, i.e. the red blood cell thickness was correlated to the hemoglobin distribution. Huang and colleagues in 2014 published a study that evaluated the possibility to combine micro-Raman spectroscopy with image analysis for label-free identification of normal spermatozoa [48]. Recently, our group proposed a similar system, which combines Raman spectroscopy/imaging and digital holography microscopy as a potential tool to rapidly and objectively identify the healthy spermatozoa [36, 49, 50].

4.1. The optical setup

The setup used in our works for the simultaneous Raman and holographic analysis essentially consists of a Raman microscope coupled to an interferometer (**Figure 5**) [36, 49, 50]. We used two different laser sources: a green laser at 532 nm for the Raman excitation and a long coherence (>100 m) red laser at 660 nm for the holographic experiments. The red laser beam was split into two beams: the object beam passing through the sample and the reference beam

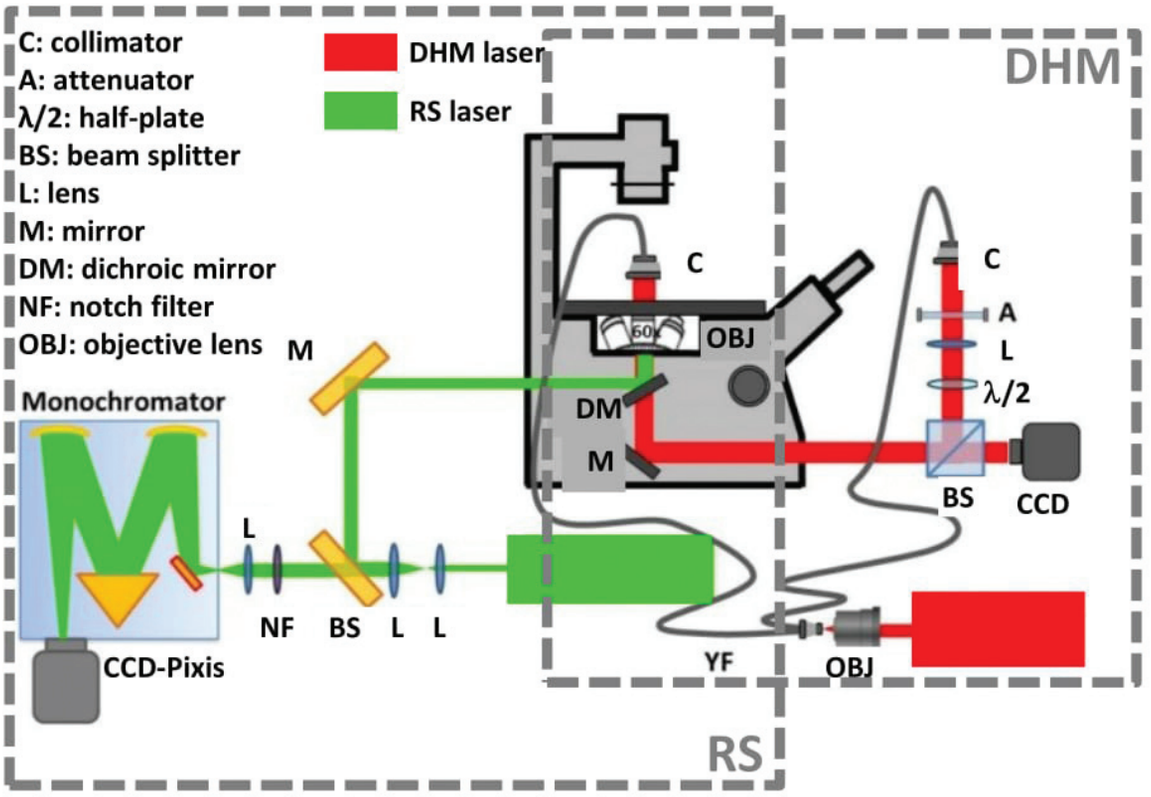

Figure 5. Experimental set up of the combined Raman and holographic system used in our works [36, 49, 50].

that directly goes to the detector. Importantly, the reference beam was controllable in intensity and polarization enabling us to improve signal intensity and contrast. The collimated object beam of the holographic pathway is recombined to the reference beam by a beam splitter (BS). The recombined beams are filtered and sent to the CCD camera (CCD1) for the holograms recording.

The green light is focused on the sample by a high numerical aperture objective lens. The high N.A. of the objective and the wavelength chosen for the Raman beam allows to reaching spatial resolutions on the order of less than 0.5 μm, particularly suitable for cell imaging application. The back-scattered light from the sample is collected by the same objective lens (OBJ) and separated from the holographic radiation by a long pass dichroic mirror (DM) reflecting wavelength below 600 nm. The scattered light, consisting of Rayleigh and Raman radiation, is filtered through a dichroic beam splitter (BS45) that rejects the Rayleigh light at 532 nm. The Raman signal is further filtered using a laser-blocking filter (NF0) to eliminate the residual Rayleigh scattering and then focused onto the entrance slit of a monochromator. The Raman signal is finally detected using a cooled CCD camera (CCD2).

4.2. Morphological and biochemical analysis of single sperm cells

In this paragraph, some of the most interesting results we have obtained by applying the Raman/holographic microscope for the sperm cell characterization will be discussed. Our investigations mainly focused on:

1. correlative analysis of morphological and biochemical alterations [49];
2. morphological and biochemical analysis of photo-damaged spermatozoa [36];
3. sex classification of bovine spermatozoa [49, 51].

With the aim of demonstrating the potential applicability of the proposed multimodal imaging approach in identifying the fertile spermatozoa for IVF, we have first performed a qualitative Raman/holographic analysis of single sperm cells [49].

Raman imaging can be performed scanning the laser over a region of interest of the sperm cell or on the entire cells, acquiring in that way a point-by-point spectrum. Similar spectral features correspond to similar molecular structures; consequently, we can identify separate regions of the spermatozoon (acrosome, nucleus, and tail) according to their different chemical composition (**Figure 6a** and **b**). Pseudo-color Raman map of the sperm is shown in **Figure 6b**, in which each color is arbitrarily associated to specific Raman spectral patterns. Therefore, the Raman map delineates not only the distribution of DNA and protein in the nucleus, acrosome and tail but also detects, in a label-free manner, small biochemical discrepancies correlated with the presence of morphological defects, highlighted by digital holography (**Figure 6c**). We found that the peculiar protuberance in the region of the spermatozoon connecting the head to the tail, the so-called middle piece, well correlated with the biochemical alteration detected in the Raman map. Indeed, by analyzing the typical Raman bands of the spectra acquired in that specific cell region, it was possible to correlate the morphological alteration to an increased amount of proteins in the middle-piece region, where mitochondria are localized [49].

Recently, we applied the multimodal imaging tool for the online evaluation of the damages induced by green laser radiation for studying in which dose and how it affects the irradiated sperm cells [36]. Severe spermatozoa variations associated with a topological redistribution of the sample and a gradual decrease in the Raman signal intensity were detected in a label-free configuration (**Figure 7a–c**). Importantly, at laser fluences (30 MJ/cm^2) where no morphological alterations were detected by digital holography, high specific spectral variations were monitored to evaluate the cell photodegradation. More specifically, Raman analysis provided precise information on the most affected biochemical structures, finding that DNA phosphate

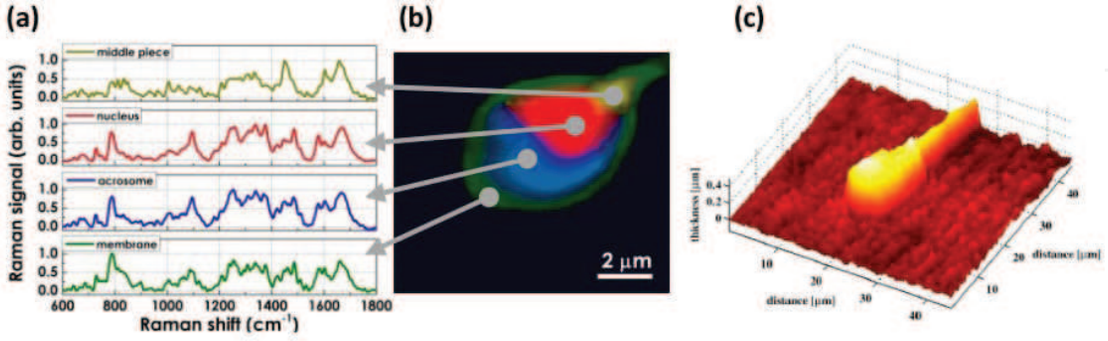

Figure 6. (a) Raman spectra and (b) false-color Raman map of different regions of the sperm cell head: middle piece (yellow), nucleus (red), acrosome (blue), and membrane (green). (c) 3D digital holographic reconstruction of the sperm cell morphology [49].

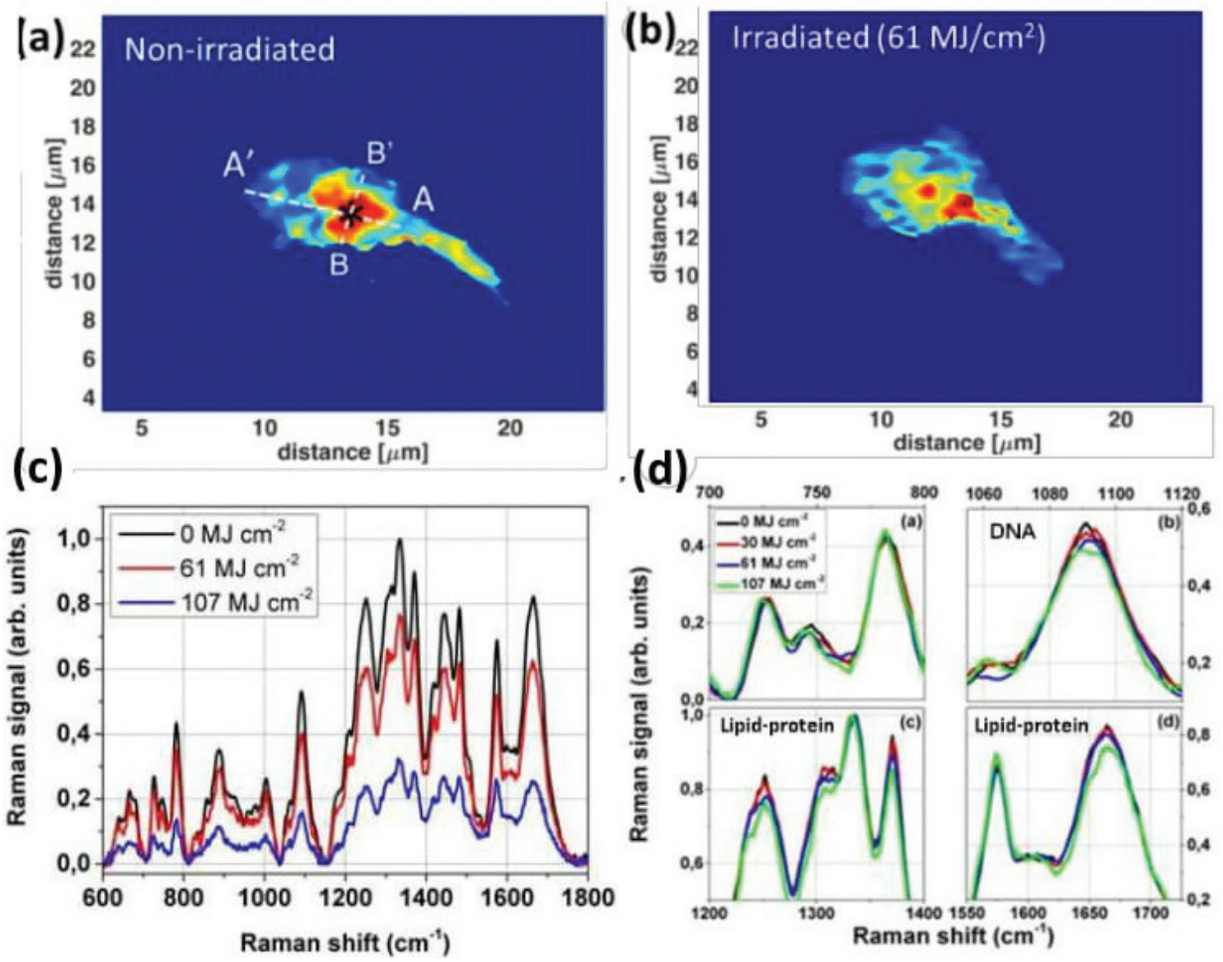

Figure 7. (Top) Reconstructed phase map of the (a) nonirradiated and (b) irradiated region of interest at the focus plane. The star (*) indicates the cell position where the Raman spectrum is acquired that corresponds to the irradiated area. (c) Raman spectra of the sperm cell at three different selected laser fluences (0, 61 and 107 MJ/cm^2). (d) Zoom of four selected Raman spectra acquired at laser fluences of 0, 30, 61 and 107 MJ/cm^2 in the spectral region between 700–800 cm^{-1}, 1050–1120 cm^{-1}, 1200–1400 cm^{-1} and 1550–1720 cm^{-1} [36].

backbone (900–1100 cm^{-1}) and lipids and proteins (1200–1400 cm^{-1}) are very sensitive to photoxidative denaturation (**Figure 7d**) [36].

To test the biochemical/morphological ability of the proposed multimodal approach, we additionally tested bovine sperm cells. The sex preselection of the offspring reveals a high significant impact on animal production management as well as genetic improvement programs. Since a noninvasive method for sex predetermination in animals is still not available, we used our multimodal approach for identifying and separating X and Y-bearing sperm cells. The key parameters estimated in our works [49, 51], on hundreds bovine spermatozoa of different bulls, were the Raman bands correlated to DNA content and head volume.

Indeed, specific peaks related to the vibrational modes of the DNA bases (726 and 785 cm^{-1}) can be used to sort X- and Y-bovine sperm cells (**Figure 8a** and **b**). However, additional significant spectral variations can be observed in the Raman bands mainly associated with the presence of lipids and proteins (1400–1600 cm^{-1}, **Figure 8a** and **b**), due to the different composition of the

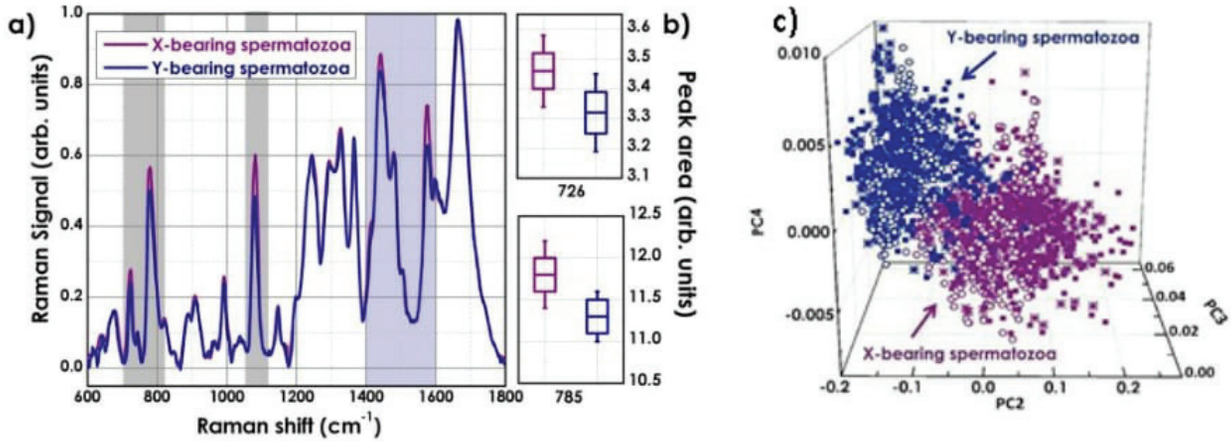

Figure 8. (a) Average Raman spectra of 900 X- (purple line) and 900 Y- (blue line) sperm cell spectra acquired in the "fingerprint" spectral region. (b) Measured peak area of the bands at 726 and 785 cm^{-1}, highlighting the different DNA content measured for X and Y sperm cells, $\Delta A = 4.2 \pm 0.9\%$. (c) PCA score plots of PC2, PC3 and PC4 showing the separation of data corresponding to X- and Y- sperm cells [49, 51].

sex-associated membrane proteins in X- and Y-bearing sperm cells. In order to quantify the efficiency and the accuracy of the Raman spectroscopy in discriminating the two sperm cell populations, we have analyzed the data using a multivariate statistical method, known as principal component analysis, that allows to visualizing the separation of the two classes of cells into two well distinct clusters (**Figure 8c**), only on the base of the differences in their Raman fingerprint. The sorting accuracy resulted of 90.6%, which is comparable to the accuracy (90–94%) achievable with standard sorting techniques such as fluorescence-activated cell sorting (FACS).

Then, the spectroscopic results have been correlated with the morphological analysis, where the sperm head volume has been evaluated by applying the Otsu's method [51] on the holographic phase map, a procedure generally used to indirectly measure morphological properties of the region under investigation (results not reported, see [49, 51]). As the main differences between X and Y chromosomes are the size (X chromosome is bigger than Y one) and the total DNA content, these major differences can be reflected in the head sperm volume, representing therefore a fast and automated way to identify the chromosome type [49, 51].

Therefore, by combining holographic with Raman microscopy provides label-free, quantitative morphological and chemical information from unfixed sperm cells. The combination offers an excellent system for a complete, morphological and physiological, monitoring of the sperm cell quality.

5. Towards clinical applications: a demanding path

Despite the feasibility of Raman spectroscopy and holography microscopies has been successfully demonstrated in many medical and biological applications [14, 16, 30, 52–55], there is still a significant lack of translation and implementation of such innovative techniques into clinical practice. Indeed, while thanks to the technological advances the capability and information achievable are quickly expanding, there are some concerns to consider [56].

The Raman signals are generally low and often obscured by the presence of the cell autofluorescence. However, the fluorescence-free detection can be achieved using instruments working in the near-IR region of the spectrum, also reducing the cell photodamage. Alternatively, modulating or multiwavelengths approaches can be employed to eliminate the fluorescence background [57–59].

Another crucial aspect for translational applications is the time required to collect the spectral data and reconstruct the Raman images. Indeed, for reproductive medicine applications, performing experiment in real-time is crucial. Recently, several approaches have been proposed providing a faster imaging modality and allowing investigation of several sperm cells simultaneously such as the Coherent anti-Stokes Raman scattering (CARS) and surface-enhanced Raman scattering (SERS) imaging [60, 61] or the use of structured illumination [62, 63]. Moreover, in our specific case, the sample is moving while measuring. This represents another problem that researchers are trying to overcome using the laser trapping capability [64, 65], slide functionalization procedures [25, 66], or microfluidic devices [67, 68].

A further obstacle to the clinical success of these new methods is the complexity in interpreting the results. Indeed, the newer instruments for Raman/holographic imaging are fast, efficient, and reliable; however, they require specialized operators. An useful system should be easier to use, providing clear and automated answers to biomedical problems instead of spectra or holograms. The ongoing implementation of computer-assisted diagnosis algorithms is helping the interpretation of the holographic images, while further work on the creation of larger Raman database is still required.

The economical aspect has also to be considered. Raman spectroscopy and digital holography use precise equipment. If we consider that a holographic imaging system is sensitive to optical pathway differences on the nanoscale and has to be isolated to any kinds of vibrations for avoiding artifacts, we can well image that the precision required in the construction of such devices is more expansive than that of conventional microscopes currently in clinical use.

The path to clinical implementation of innovative multimodal imaging techniques for sperm cell assessment passes through the following milestones: 1. identification of the medical problem and the need for a new technique; 2. experimental tests of the technique, showing the proof of principle and the feasibility of the specific application; 3. closely collaboration between researchers and clinicians for evaluating the clinical relevance of the information the new technique provides; 4. optimisation of the technique for the specific application in order to improve its sensibility, specificity and robustness; 5. clinical trials; 6. industrial implementation of the system for making it clinician and patient friendly; and 7. Clinical implementation.

The proof of principle of Raman spectroscopy and holographic imaging as sperm selection techniques has been successfully demonstrated. Their use for detecting epigenetic alterations, including DNA packaging and spatial conformation, methylation, and histone modification, that could seriously affect the embryonic development has been showed [21]. Researches in this field are currently focusing on the points 3 and 4, as highlighted in this chapter. Our efforts aim to assess the feasibility and the reliability of the two techniques before initiating the clinical trials, filling in such a way the gap between experimentation and clinical implementation.

Author details

Annalisa De Angelis[1]*, Maria Antonietta Ferrara[2], Giuseppe Coppola[2] and Anna Chiara De Luca[1]

*Address all correspondence to: a.deangelis@ibp.cnr.it

1 Institute of Protein Biochemistry - National Research Council, Naples, Italy

2 Institute for Microelectronics and Microsystems - National Research Council, Naples, Italy

References

[1] Cooper TG, Noonan E, von Eckardstein S, Auger J, Baker HWG, Behre HM, et al. World Health Organization reference values for human semen characteristics. Human Reproduction Update. 2009;**00**(0):1-15

[2] Mortimer ST. CASA—Practical aspects. Journal of Andrology. 2000;**21**(4):515-524

[3] Hirano Y, Shibahara H, Obara H, Suzuki T, Takamizawa S, Yamaguchi C, et al. Andrology: Relationships between sperm motility characteristics assessed by the computer-aided sperm analysis (CASA) and fertilization rates in vitro. Journal of Assisted Reproduction and Genetics. 2001;**18**(4):215-220

[4] Zaini A, Jennings MG, Baker HWG. Are conventional sperm morphology and motility assessments of predictive value in subfertile men? International Journal of Andrology. 1985 Dicembre;**8**(6):427-435

[5] Avendaño C, Oehninger S. DNA fragmentation in morphologically normal spermatozoa: How much should we be concerned in the ICSI era? Journal of Andrology. 2011 Jul 8;**32**(4):356-363

[6] Sharma R, Masaki J, Agarwal A. Sperm DNA fragmentation analysis using the TUNEL assay. In: Spermatogenesis: Methods and Protocols. 2013;**927**:121-136

[7] Simon L, Lutton D, McManus J, Lewis SE. Sperm DNA damage measured by the alkaline Comet assay as an independent predictor of male infertility and in vitro fertilization success. Fertility and Sterility. 2011;**95**(2):652-657

[8] Fernández JL, Muriel L, Goyanes V, Segrelles E, Gosálvez J, Enciso M, et al. Simple determination of human sperm DNA fragmentation with an improved sperm chromatin dispersion test. Fertility and Sterility. 2005;**84**(4):833-842

[9] Evenson DP. Sperm chromatin structure assay (SCSA®). In: Spermatogenesis: Methods and Protocols. 2013;**927**:147-164

[10] Sánchez V, Wistuba J, Mallidis C. Semen analysis: Update on clinical value, current needs and future perspectives. Reproduction. 2013;**146**(6):R249-R258

[11] Henkel R, Kierspel E, Hajimohammad M, Stalf T, Hoogendijk C, Mehnert C, et al. DNA fragmentation of spermatozoa and assisted reproduction technology. Reproductive Biomedicine Online. 2003;**7**(4):477-484

[12] Notingher I. Raman spectroscopy cell-based biosensors. Sensors. 2007;**7**(8):1343-1358

[13] Chang L, LoBiondo JG. Setup of micromanipulator for sperm selection and injection for IMSI: Configuring the microscope for intracytoplasmic morphology-selected sperm injection (IMSI). In: Agarwal A, Borges Jr E, Setti A. (eds) Non-Invasive Sperm Selection for In Vitro Fertilization. Springer, New York, NY; 2015. p. 91-103 https://doi.org/10.1007/978-1-4939-1411-1_9

[14] Haifler M, Girshovitz P, Band G, Dardikman G, Madjar I, Shaked NT. Interferometric phase microscopy for label-free morphological evaluation of sperm cells. Fertility and Sterility. 2015 Luglio;**104**(1):43-47.e2

[15] Coppola G, Caprio GD, Wilding M, Ferraro P, Esposito G, Matteo LD, et al. Digital holographic microscopy for the evaluation of human sperm structure. Zygote. 2014 Nov;**22**(4):446-454

[16] Gianaroli L, Magli MC, Ferraretti AP, Crippa A, Lappi M, Capitani S, et al. Birefringence characteristics in sperm heads allow for the selection of reacted spermatozoa for intracytoplasmic sperm injection. Fertility and Sterility. 2010;**93**(3):807-813

[17] De Angelis A, Ferrara MA, Di Caprio G, Managò S, Sirleto L, Coppola G, et al. A combined holographic and Raman microscopy approach for the assessment of spermatozoa. In: Fotonica AEIT Italian Conference on Photonics Technologies, 6-8 May 2015; Turin, Italy: IET Digital Library; 2015. p. 1- 4

[18] Puppels GJ, de Mul FFM, Otto C, Greve J, Robert-Nicoud M, Arndt-Jovin DJ, et al. Studying single living cells and chromosomes by confocal Raman microspectroscopy. Nature. 1990 Sep 20;**347**(6290):301-303

[19] Majzner K, Kaczor A, Kachamakova-Trojanowska N, Fedorowicz A, Chlopicki S, Baranska M. 3D confocal Raman imaging of endothelial cells and vascular wall: Perspectives in analytical spectroscopy of biomedical research. The Analyst. 2013;**138**(2):603-610

[20] Kubasek WL, Wang Y, Thomas GA, Patapoff TW, Schoenwaelder KH, Van der Sande JH, et al. Raman spectra of the model B-DNA oligomer d (CGCGAATTCGCG) 2 and of the DNA in living salmon sperm show that both have very similar B-type conformations. Biochemistry (Moscow). 1986;**25**(23):7440-7445

[21] Huser T, Orme CA, Hollars CW, Corzett MH, Balhorn R. Raman spectroscopy of DNA packaging in individual human sperm cells distinguishes normal from abnormal cells. Journal of Biophotonics. 2009;**2**(5):322

[22] Rajender S, Avery K, Agarwal A. Epigenetics, spermatogenesis and male infertility. Mutation Research. 2011;**727**(3):62-71

[23] Meister K, Schmidt DA, Bründermann E, Havenith M. Confocal Raman microspectroscopy as an analytical tool to assess the mitochondrial status in human spermatozoa. The Analyst. 2010;**135**(6):1370-1374

[24] Mallidis C, Wistuba J, Bleisteiner B, Damm OS, Gross P, Wübbeling F, et al. In situ visualization of damaged DNA in human sperm by Raman microspectroscopy. Human Reproduction. 2011;**26**(7):1641-1649

[25] Sánchez V, Redmann K, Wistuba J, Wübbeling F, Burger M, Oldenhof H, et al. Oxidative DNA damage in human sperm can be detected by Raman microspectroscopy. Fertility and Sterility. 2012;**98**(5):1124-1129

[26] Edengeiser E, Meister K, Bründermann E, Büning S, Ebbinghaus S, Havenith M. Non-invasive chemical assessment of living human spermatozoa. RSC Advances. 2015;**5**(14): 10424-10429

[27] Barry H, Okezie IA. DNA and Free Radicals. England: Ellis Horwood Limited; 1993

[28] Shamsi MB, Imam SN, Dada R. Sperm DNA integrity assays: Diagnostic and prognostic challenges and implications in management of infertility. Journal of Assisted Reproduction and Genetics. 2011;**28**(11):1073-1085

[29] Arnison MR, Larkin KG, Sheppard CJ, Smith NI, Cogswell CJ. Linear phase imaging using differential interference contrast microscopy. Journal of Microscopy. 2004;**214**(1):7-12

[30] Zernike F. Phase contrast, a new method for the microscopic observation of transparent objects. Physica. 1942;**9**(7):686-698

[31] Balberg M, Levi M, Kalinowski K, Barnea I, Mirsky SK, Shaked NT. Localized measurements of physical parameters within human sperm cells obtained with wide-field interferometry. Journal of Biophotonics. 2017 Gennaio;n/a-n/a

[32] Schnars U, Jüptner W. Direct recording of holograms by a CCD target and numerical reconstruction. Applied Optics. 1994;**33**(2):179-181

[33] Yu L, Cai L. Iterative algorithm with a constraint condition for numerical reconstruction of a three-dimensional object from its hologram. JOSA A. 2001;**18**(5):1033-1045

[34] Goodman JW. Introduction to Fourier Optics. Roberts and Company Publishers. 3rd ed. Greenwood Village, CO; 2005. 520 p

[35] Nazarathy M, Shamir J. Fourier optics described by operator algebra. JOSA. 1980;**70**(2): 150-159

[36] Ferrara MA, De Angelis A, De Luca AC, Coppola G, Dale B, Coppola G. Simultaneous holographic microscopy and Raman spectroscopy monitoring of human spermatozoa photodegradation. IEEE Journal of Selected Topics in Quantum Electronics. 2016;**22**(3):1-8

[37] Ferrara MA, Dardano P, De Stefano L, Rea I, Coppola G, Rendina I, et al. Optical properties of diatom nanostructured biosilica in *Arachnoidiscus* sp: Micro-optics from mother nature. PLoS One. 2014;**9**(7):e103750

[38] Mico V, Zalevsky Z, Ferreira C, García J. Superresolution digital holographic microscopy for three-dimensional samples. Optics Express. 2008;**16**(23):19260-19270

[39] Haifler M, Girshovitz P, Band G, Dardikman G, Madjar I, Shaked NT. Interferometric phase microscopy for label-free morphological evaluation of sperm cells. Fertility and Sterility. 2015;**104**(1):43-47

[40] Guerrero A, Carneiro J, Pimentel A, Wood CD, Corkidi G, Darszon A. Strategies for locating the female gamete: The importance of measuring sperm trajectories in three spatial dimensions. MHR: Basic Science of Reproductive Medicine. 2011;**17**(8):511-523

[41] Di Caprio G, Gioffre MA, Saffioti N, Grilli S, Ferraro P, Puglisi R, et al. Quantitative label-free animal sperm imaging by means of digital holographic microscopy. IEEE Journal of Selected Topics in Quantum Electronics. 2010;**16**(4):833-840

[42] Di Caprio G, Ferrara MA, Miccio L, Merola F, Memmolo P, Ferraro P, et al. Holographic imaging of unlabelled sperm cells for semen analysis: A review. Journal of Biophotonics. 2015;**8**:779-789

[43] Coppola G, Di Caprio G, Wilding M, Ferraro P, Esposito G, Di Matteo L, et al. Digital holographic microscopy for the evaluation of human sperm structure. Zygote. 2014; **22**(4):446-454

[44] Merola F, Miccio L, Memmolo P, Di Caprio G, Galli A, Puglisi R, et al. Digital holography as a method for 3D imaging and estimating the biovolume of motile cells. Lab on a Chip. 2013;**13**(23):4512-4516

[45] Shaked NT, Satterwhite LL, Rinehart MT, Wax A. Quantitative analysis of biological cells using digital holographic microscopy. In: Joseph Rosen, editor. Holography, Research and Technologies. InTech; 2011. p. 219-236

[46] Di Caprio G, El Mallahi A, Ferraro P, Dale R, Coppola G, Dale B, et al. 4D tracking of clinical seminal samples for quantitative characterization of motility parameters. Biomedical Optics Express. 2014;**5**(3):690-700

[47] Kang JW, Lue N, Kong C-R, Barman I, Dingari NC, Goldfless SJ, et al. Combined confocal Raman and quantitative phase microscopy system for biomedical diagnosis. Biomedical Optics Express. 2011;**2**(9):2484-2492

[48] Huang Z, Chen G, Chen X, Wang J, Chen J, Lu P, et al. Rapid and label-free identification of normal spermatozoa based on image analysis and micro-Raman spectroscopy. Journal of Biophotonics. 2014;**7**(9):671-675

[49] Ferrara MA, Di Caprio G, Managò S, De Angelis A, Sirleto L, Coppola G, et al. Label-free imaging and biochemical characterization of bovine sperm cells. Biosensors. 2015;**5**(2):141-157

[50] De Angelis A, Managò S, Ferrara MA, Napolitano M, Coppola G, De Luca AC. Combined Raman spectroscopy and digital holographic microscopy for sperm cell quality analysis. Journal of Spectroscopy. 2017;**2017**:1-14

[51] De Luca AC, Managó S, Ferrara MA, Rendina I, Sirleto L, Puglisi R, et al. Non-invasive sex assessment in bovine semen by Raman spectroscopy. Laser Physics Letters. 2014;**11**(5):055604

[52] Otsu N. A threshold selection method from gray-level histograms. Automatica. 1975;**11** (285–296):23-27

[53] Harz M, Rösch P, Popp J. Vibrational spectroscopy—A powerful tool for the rapid identification of microbial cells at the single-cell level. Cytometry. Part A. 2009;**75**(2):104-113

[54] Li M, Xu J, Romero-Gonzalez M, Banwart SA, Huang WE. Single cell Raman spectroscopy for cell sorting and imaging. Current Opinion in Biotechnology. 2012;**23**(1):56-63

[55] Managò S, Valente C, Mirabelli P, Circolo D, Basile F, Corda D, et al. A reliable Raman-spectroscopy-based approach for diagnosis, classification and follow-up of B-cell acute lymphoblastic leukemia. Scientific Reports. 2016;**6**:24821

[56] Webb SJ. Laser-Raman spectroscopy of living cells. Physics Reports. 1980;**60**(4):201-224

[57] Canetta E, Mazilu M, De Luca AC, Carruthers AE, Dholakia K, Neilson S, et al. Modulated Raman spectroscopy for enhanced identification of bladder tumor cells in urine samples. Journal of Biomedical Optics. 2011;**16**(3):037002-037002

[58] De Luca AC, Mazilu M, Riches A, Herrington CS, Dholakia K. Online fluorescence suppression in modulated Raman spectroscopy. Analytical Chemistry. 2009;**82**(2):738-745

[59] De Luca AC, Dholakia K, Mazilu M. Modulated Raman spectroscopy for enhanced cancer diagnosis at the cellular level. Sensors. 2015;**15**(6):13680-13704

[60] Li L, Wang H, Cheng J-X. Quantitative coherent anti-Stokes Raman scattering imaging of lipid distribution in coexisting domains. Biophysical Journal. 2005;**89**(5):3480-3490

[61] Zito G, Rusciano G, Pesce G, Dochshanov A, Sasso A. Surface-enhanced Raman imaging of cell membrane by a highly homogeneous and isotropic silver nanostructure. Nanoscale. 2015;**7**(18):8593-8606

[62] De Luca AC, Reader-Harris P, Mazilu M, Mariggio S, Corda D, Di Falco A. Reproducible surface-enhanced Raman quantification of biomarkers in multicomponent mixtures. ACS Nano. 2014;**8**(3):2575-2583

[63] Kosmeier S, Zolotovskaya S, De Luca AC, Riches A, Herrington CS, Dholakia K, et al. Nonredundant Raman imaging using optical eigenmodes. Optica. 2014;**1**(4):257-263

[64] De Luca AC, Kosmeier S, Dholakia K, Mazilu M. Optical eigenmode imaging. Physical Review A. 2011 Aug 15;**84**(2):021803

[65] Di Caprio G, Ferrara MA, Miccio L, Merola F, Memmolo P, Ferraro P, et al. Holographic imaging of unlabelled sperm cells for semen analysis: A review. Journal of Biophotonics. 2015 Oct 1;**8**(10):779-789

[66] De Luca AC, Rusciano G, Ciancia R, Martinelli V, Pesce G, Rotoli B, et al. Spectroscopical and mechanical characterization of normal and thalassemic red blood cells by Raman tweezers. Optics Express. 2008;**16**(11):7943-7957

[67] Frimat J-P, Bronkhorst M, de Wagenaar B, Bomer JG, Van der Heijden F, Van den Berg A, et al. Make it spin: Individual trapping of sperm for analysis and recovery using micro-contact printing. Lab on a Chip. 2014;**14**(15):2635-2641

[68] De Wagenaar B, Berendsen JTW, Bomer JG, Olthuis W, van den Berg A, Segerink LI. Microfluidic single sperm entrapment and analysis. Lab on a Chip. 2015;**15**(5):1294-1301

IntechOpen